Available online at www.sciencedirect.com

ScienceDirect

Advances in Space Research 66 (2020) 116–134

ADVANCES IN SPACE RESEARCH (a COSPAR publication)

www.elsevier.com/locate/asr

# IDEASSat: A 3U CubeSat mission for ionospheric science

Yi Duann [a], Loren C. Chang [a,*], Chi-Kuang Chao [a], Yi-Chung Chiu [a], Rong Tsai-Lin [a], Tzu-Ya Tai [a], Wei-Hao Luo [a], Chi-Ting Liao [a], Hsin-Tzu Liu [a], Chieh-Ju Chung [a], Ru Duann [a], Cheng-Ling Kuo [a], Jann-Yenq Liu [a], Zhe-Ming Yang [a], Glenn Franco Gacal [a], Amal Chandran [b,d], Hari Priyardarshan [c], Ankit Verma [c], Tzu-Wei Fang [d,e], Sarthak Srivastava [d]

[a] *Center for Astronautical Physics and Engineering, Institute of Space Science and Engineering, National Central University, Taiwan*
[b] *Laboratory for Atmospheric and Space Physics, University of Colorado at Boulder, Boulder, CO, USA*
[c] *Department of Avionics, Indian Institute of Space Science and Technology, Kerala, India*
[d] *Satellite Research Centre, Nanyang Technological University, Singapore*
[e] *CIRES/University of Colorado at Boulder, Boulder, CO, USA*

Received 30 August 2019; received in revised form 6 January 2020; accepted 13 January 2020
Available online 29 January 2020

**Abstract**

The Ionospheric Dynamics Exploration and Attitude Subsystem Satellite (IDEASSat/ INSPIRESat-2) is a three-unit (U) CubeSat developed with the objective of providing in-situ measurements of the Earth's ionosphere in order to quantify both global scale ionospheric variability and small scale irregularities. The science payload is the Compact Ionospheric Probe (CIP) - an all in one in-situ plasma sensor developed at Taiwan National Central University (NCU), which is the miniaturized version of the larger Advanced Ionospheric Probe (AIP) that is carried and operational aboard the 450 kg FORMOSAT-5 spacecraft. The spacecraft has been developed by NCU in partnership with the International Satellite Program in Research and Education (INSPIRE) consortium, and is funded by the Taiwan National Space Organization (NSPO), Ministry of Science and Technology, and Ministry of Education as part of the first national effort to encourage small satellite development at Taiwan universities. The development of IDEASSat offers students a hands-on opportunity to learn about space science and technology and will work in conjunction with FORMOSAT-5 and INSPIRESat-1 to provide ionospheric observations spanning different altitudes and local times. The IDEASSat spacecraft subsystems are a combination of commercial off the shelf (COTS) and self-developed components designed by NCU in partnership with other INSPIRE member universities. IDEASSat is expected to be launched in late 2020. In this report, we describe the IDEASSat mission and spacecraft design, as well as unique lessons learned as part of the development process.


*Keywords:* Cubesat; Ionosphere; Capacity building

## 1. Introduction

Since the first CubeSats were launched in mid 2003, they have ushered in a new epoch in human space history in offering reduced cost access to the space for nontraditional players. A smaller size spacecraft with reduced complexity and standardized specifications offers the chance to

* Corresponding author.
*E-mail addresses:* cntwtpe@g.ncu.edu.tw (Y. Duann), loren@g.ncu.edu.tw (L.C. Chang), ckchao@jupiter.ss.ncu.edu.tw (C.-K. Chao), clkuo@jupiter.ss.ncu.edu.tw (C.-L. Kuo), jyliu@jupiter.ss.ncu.edu.tw (J.-Y. Liu), glenn.gacal@obf.ateneo.edu (G.F. Gacal), achandran@ntu.edu.sg (A. Chandran), priyadarshnam@iist.ac.in (H. Priyardarshan), tzu-wei.fang@noaa.gov (T.-W. Fang), sarthak.s@ntu.edu.sg (S. Srivastava).

https://doi.org/10.1016/j.asr.2020.01.012
0273-1177/

understand the operation and interfaces of subsystems, providing a great opportunity for student education. CubeSats allow students to develop a full spacecraft in a period as short as 2 years, with a much lower price compared to larger satellites. After almost two decades, it has become more and more common to see CubeSats in project-based learning class, and the miniaturized components are sold by a large variety of companies. At this stage of development, CubeSats are not only an educational tool, but also a viable platform to perform scientific measurements.

The International Satellite Program in Research and Education (INSPIRE) consortium was formed in 2015, with the objectives of developing small satellites to perform science missions, building a project-based learning curriculum for space science and engineering, and establishing a supporting network of ground stations. The consortium was initially comprised of the University of Colorado at Boulder (CU), National Central University in Taiwan (NCU), and the Indian Institute of Space Science and Technology (IIST). The consortium has since expanded to eleven institutions as of 2019, with six small satellite science missions funded from sources secured by the participating institutions (Baker and Chandran, 2018; Chang et al., 2018b). A large number of these missions are focused upon the study of the Earth's upper atmosphere, including the neutral thermosphere (~90 - above 500 km altitude) and mesosphere (~60–90 km), as well as the ionosphere (~60–1000 km).

The ionosphere is the ionized part of the upper atmosphere, formed by the photoionization of neutral atmosphere in the mesosphere and thermosphere through absorption of solar extreme ultraviolet (EUV) and X-ray radiation. There are strong day-night differences as well as day-to-day, seasonal, and solar cycle variability in the ionosphere. Changes in the ionosphere affect radio propagation and Global Navigation Satellite System (GNSS) signals. High frequency (HF) radio transmissions propagating obliquely into the ionosphere can be refracted over the horizon for long distance communications or surveillance purposes (Frissell et al., 2014). Ionospheric plasma can also cause electrical charging of spacecraft flying in the space.

Modern society relies heavily upon terrestrial and satellite radio communications that are affected by the ionosphere. Trans-ionospheric radio signals, such as those from Global Navigation Satellite Systems (GNSS) are refracted by ionospheric plasma, introducing time and range errors proportional to the integrated electron content along the propagation path (Zhong et al., 2008). Smaller scale irregularities in plasma distribution such as plasma bubbles and Travelling Ionospheric Disturbances (TIDs) can diffract GNSS signals, resulting in scintillation and signal fading at the receiver end, which can render the signal unusable (Afraimovich et al., 2004). Terrestrial high frequency (HF) radio transmissions are also refracted and reflected by ionospheric plasma allowing for over the horizon communications and surveillance (Daniel et al., 2016). Measurement of ionospheric plasma parameters at planetary scales, with sampling frequency high enough to resolve small scales irregularities is therefore crucial for understanding ionospheric variability and its effects on human technology.

This paper focuses on the mission objectives and design of the Ionospheric Dynamics Exploration and Attitude Subsystem Satellite (IDEASSat/ INSPIRESat-2) - a CubeSat that is designed to measure and study planetary-scale wave structures in the ionosphere, the distribution of ionospheric irregularities and Travelling Ionospheric Disturbances (TIDs), as well as the electric fields driving vertical plasma drifts, and their relation to the ionospheric *F* region wind dynamo.

## 2. Mission overview

The Ionospheric Dynamics Exploration and Attitude Subsystem Satellite (IDEASSat/ INSPIRESat-2, hereafter referred to as IDEASSat) is a 3U CubeSat whose development began as one of the missions in the International Satellite Program in Research and Education (INSPIRE) consortium in May 2017 (Chang et al., 2018a). As shown in the Science Traceability Matrix (Table 1), the primary objectives of this mission are (1) Measuring planetary-scale wave structures in the ionosphere, and quantifying their variability and contribution to ionospheric morphology; (2) Measuring the distribution, and structure of ionospheric irregularities and Travelling Ionospheric Disturbances (TIDs); (3) Inferring the electric fields driving vertical plasma drifts, and their relation to the ionospheric *F* region wind dynamo. The corresponding measurement and functional requirements imposed upon the ionospheric science mission by these objectives, as well as the payload will be further described in the following sections. A secondary mission involving the capture of star tracker images for attitude determination algorithm tests is specified in Table 2 and will be performed. This report focuses upon the primary ionospheric science mission.

IDEASSat has been funded with support from the Taiwan National Space Organization (NSPO), Ministry of Science and Technology, and Ministry of Education. Fig. 1 shows the engineering model (EM) prototype of IDEASSat that was fabricated in April 2019 as part of a fit check for the spacecraft components. Fabrication and integration of the flight model (FM) was initiated in May 2019, and is scheduled to be launched on the Indian Polar Satellite Launch Vehicle (PSLV - ISILaunch) in late 2020. The IDEASSat FM will have an expected one year life time in a 500 km Sun-synchronous orbit (SSO, 97.41° inclination) with a local time of descending node (LTDN) between 10:00 and 12:00. This is close to the 720 km orbital plane of the FORMOSAT-5 with LTDN at 10:30, allowing for observations at different altitudes within this local time sector. This section provides an overview of the ionospheric science objectives and its relation to other recent and ongoing ionospheric science missions.

Table 1
IDEASSat Primary Science Traceability Matrix (1).

| Science Traceability Matrix (1) | | |
|---|---|---|
| Science Objectives | Objectives<br>Measurement | Measurement Requirements (Capabilities) |
| S1. To measure planetary- scale wave structures in the ionosphere, and quantify their variability and contribution to ionospheric morphology.<br>S2. To measure the distribution, occurrence rate, and structure of ionospheric irregularities and Travelling Ionospheric Disturbances (TIDs).<br>S3. To infer the electric fields driving vertical plasma drifts, and their relation to the ionospheric *F* region wind dynamo. | Ionospheric parameters in the F-region (400 ~ 600 km altitude).<br>20 km (100 km) horizontal sampling resolution.<br>Latitude range exceeding ±30°.<br>400 ~ 600 km orbital plane in quadrature or parallel with DMSP/ FORMOSAT-5.<br>Likely 0930 ~ 1030.<br>Observations for at least six months. | Horizontal resolution: At least 0.5x the horizontal scale of a typical plasma bubble.<br>Orbit:<br>Pointing knowledge (<0.1°).<br>Pointing stability (<0.5°). Lifetime: 6 months |
| Instrumentation | Instrument Requirements (Capabilities) | Data Processing Requirements (Capabilities) |
| Compact Ionosphere Probe (CIP) | 90degr FOV.<br>Power: <5 W<br>Pointing Accuracy:<br>Ram pointing, <0.5degr<br>Pointing Knowledge: <0.1degr<br>Science Data Packet Size:280 bytes/ packet | Onboard Storage (1 month of data): >5 GB<br>Daily Downlink:<br>24.8 MB/day, 1 raw data packet per second, full mode cycle per 3 s (4.6 MB/day, if sampled as 1 raw data packet per 15 s). |

### 2.1. Science objectives

The ionosphere and its effects on human technology have been the subject of several past and ongoing satellite missions. In this section, we briefly summarize some of these recent missions and how IDEASSat serves to complement and extend these observations. Table 3 lists a selection of ionospheric satellite missions using in-situ instruments over the past 20 years (Yeh et al., 1999; Reigber et al., 1999; Le et al., 2003; Gwal et al., 2005; Rodrigues et al., 2009; Lin et al., 2017). Though more limited in observational coverage than remote sensing methods, using the in-situ instruments to measure from close range, without complicated calibration of large distance and angle projections inherent in remote sensing missions, decreases measurement uncertainties and results in higher resolution (Teillet et al., 2003). In-situ instruments sample along the spacecraft orbit. The ionosphere is highly variable with local time, latitude and altitude, making the inclination and altitude of the spacecraft orbit, as well as the choice of a Sun-synchronous or non-Sun-synchronous orbit crucial in determining the region to be sampled. Many in-situ sensors, such as retarding potential analyzers, and Langmuir probes perform measurements through current sensors exposed to ionospheric plasma at various electric potentials, forming an I-V curve (Reifman and Dow, 1949). A complete I-V curve is required in order to derive specific ionospheric plasma parameters, such as ion and electron density and temperature (Merlino, 2007).

The Ionospheric Plasma and Electrodynamics Instrument (IPEI) was developed by the University of Texas at Dallas. The IPEI was carried by FORMOSAT-1 (also known as ROCSAT-1) satellite (Su et al., 2001), launched in 1999 into an orbit of 588 × 601 km, with 35° inclination angle. IPEI consisted of four sensors: A Retarding Potential Analyzer (RPA), two Ion Drift Meters (IDM), and an Ion Trap (IT), to measure the ion concentration, ion temperature, ram velocity, and arrival angle of the incoming ions. In 100% duty cycle, the IT can measure ion saturation currents at a sampling rate of up to 1024 Hz (Yeh et al., 1999), and the data package sampling rate is up to 16 Hz. Considering the orbital velocity in low Earth orbit (LEO), the IPEI was capable of sub-kilometer spatial resolution.

Since then, there have been several missions launched to perform in-situ measurements of the ionosphere. In 2000, the Challenging Minisatellite Payload (CHAMP) mission was launched into non sun-synchronous polar orbit at 450 km, carrying a Planar Langmuir Probe (PLP) and a Digital Ion Drift Meter (DIDM) payload provided by the U.S. Air Force Research Laboratory (AFRL). The DIDM operated with a measurement sampling rate of up to 15 Hz, measuring magnitude and direction of the incoming ion flux (Reigber et al., 2001), and the data package sampling rate is 16 Hz. In 2003, the Defense Meteorological Satellite Program (DMSP) F-16 spacecraft carried a thermal plasma instrument, the Special Sensor to measure Ions, Electrons,

Table 2
IDEASSat Secondary Science Traceability Matrix (2).

| Science Traceability Matrix (2) | | |
|---|---|---|
| Science Objectives | Objectives<br>Measurement | Measurement Requirements (Capabilities) |
| E1. To collect Star tracker images from Attitude Determination and Control Subsystem (ADCS). | Spacecraft attitude and angular velocities.<br>Spacecraft position and time.<br>Star tracker imagery. | Operation during eclipse.<br>Campaign to be performed when scheduling and power requirements allow. |
| Instrumentation | Instrument Requirements (Capabilities) | Data Processing Requirements (Capabilities) |
| GPS<br>Blue Canyon Technologies (BCT) XACT ADCS module | Image Size: 2.811 MB<br>Volume: 1U.<br>Mass: 500 g.<br>Chassis Aperture: 25 mm.<br>FOV: 7 degrees. | Attitude Determination Experiment: Daily Downlink : 12.05 MB/day |

and Scintillation-3 (SSIES-3), to an 833 km SSO along the 20:03 local time sector. The SSIES-3 observed ambient electron density and temperatures, ion density, average ion temperature and molecular weight at the satellite altitude (Kihn et al., 2006). The IDM in the SSIES-3 package sampled at the rate of 6 Hz, while the ion density was sampled at 24 Hz resolution. (Le et al., 2003). The Detection of Electromagnetic Emissions Transmitted from Earthquake Regions (DEMETER) mission was launched in 2004, to a 710 km SSO along local time 22:15 sector, with Instrument d'Analyse du Plasma (IAP) to observe and characterize the state of the ionospheric plasma and detect perturbations (Berthelier et al., 2006). The data packages are sampled at a rate of 2.7 Hz, the ion density fluctuations were measured at a sampling frequency of up to about 160 Hz, and provided a complete set of plasma parameters every ~360 ms (Gwal et al., 2005). In 2008, the Communications/Navigation Outage Forecasting System (C/NOFS) mission carrying the Ion Velocity Meter (IVM), Planar Langmuir Probe (PLP), Neutral Wind Meter (NWM), the C/NOFS Occultation Receiver for Ionospheric Sensing and Specification (CORISS), the Coherent Electromagnetic Radio Tomography (CERTO), and Vector Electric Field Instrument (VEFI) was launched. C/NOFS is measuring the in-situ ion velocity vector, ion temperature, and ion composition. The PLP and VEFI are with a measurement sampling rate up to 512 Hz at an elliptical orbit with altitude extrema varying from between 400 and 138 × 850 km, before finally de-orbiting (Rodrigues et al., 2009), while the RPA in the IVM had a nominal sampling rate of 2 Hz for a complete I-V curve (Stoneback et al., 2011). With a similar Sun-Synchronous Orbit and local time sector as DEMETER, FORMOSAT-5 was launched in 2017 carrying the Advanced Ionospheric Probe (AIP). Intended as a follow-on to FORMOSAT-1 IPEI, the AIP is an all in one in-situ plasma sensor containing RPA, IDM, PLP, and IT operating modes with a current reading rate of up to 8192 Hz. The data package sampling rate varies for different operating modes. In the nominal mode it is 1 package (1024 bytes) per 3 s, the fast mode sampling rate is 8 times that of nominal mode, and the burst mode is 64 times that of nominal mode. At the time of launch, AIP was one of the lightest and fastest sampling rate payloads to perform in-situ measurement of ionosphere physical parameters (Lin et al., 2017).

The science payload carried by IDEASSat is the Compact Ionospheric Probe (CIP) - an all in one in-situ plasma sensor developed at Taiwan National Central University (NCU), which is the miniaturized version of AIP. Intended for use aboard small satellites, the CIP is being carried aboard the INSPIRESat-1 and IDEASSat/INSPIRESat-2 small satellite missions, both of which will be delivered for launch by February 2020 and May 2020, respectively (Evonosky et al., 2018b). Both spacecraft will be launched into 500 km orbits. IDEASSat will be launched into an SSO, while the inclination of INSPIRESat-1 has not yet been finalized.

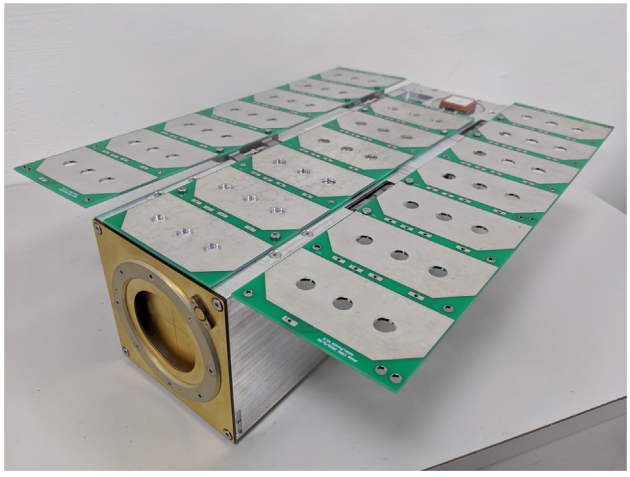

Fig. 1. The IDEASSat engineering model prototype unit.

### 2.2. Plasma irregularities and Traveling Ionospheric Disturbances

Smaller scale irregularities in the ionosphere can diffract trans-ionospheric radio signals used for satellite navigation or communications, causing rapid fluctuations in the received signal to noise ratio - a phenomena known as scintillation. Severe scintillation can render satellite communications and global navigation satellite systems (GNSS) unusable (Kelly et al., 2014). There are several types of plasma irregularities occurring in the ionosphere. Plasma bubbles are associated with density depletion, while blobs are related to density enhancement (Kil et al., 2015). Plasma bubbles occur during the nighttime, when less dense plasma at lower altitudes, caused by higher recombination rates, rises to the denser plasma above it. The physical mechanism that leads to plasma bubbles are largely attributed to the Rayleigh-Taylor instability, which is triggered when a positive vertical density gradient exists at the interface of two fluids, similar to water placed on top of oil. Plasma bubbles form around the magnetic equator in the early evening, when there is a vertical density gradient associated with the vertical plasma drift (Kil, 2015). During their vertical drift, the magnetic field aligned bubbles, also extend their extremities to higher latitudes (Sultan, 1996). The structures of bubbles can be hundreds of kilometers across in longitude and extend hundreds of kilometers up in altitude above the *F*-layer (Kil, 2015), and can transport along magnetic field lines to higher latitudes far from their initiation site. The 3-dimensional simulation of plasma plume by Retterer (2010) showed that the equatorial plasma could rise in height by 200 km in 7.8 min, the vertical growth rate being 427 m/s, which means that to study the growth process of plasma irregularities, a high measurement sampling rate is required. Plasma bubbles are identifiable in in-situ ion density measurements as sharp drops from the background plasma. A single satellite passing through a plasma bubble will garner a 1-D spatial perspective of the bubbles shape and size at some instant in time.

The traveling ionospheric disturbances (TIDs) are identified as propagating perturbations in the ionospheric electron density (Fedorenko et al., 2013), and they can be detected in the night airglow emission variation (Ogawa et al., 2001). TIDs can be driven by propagating acoustic gravity waves (AGWs) in the upper atmosphere that perturb the ionospheric electron density. Based on the phase velocity and wavelength, TIDs are often classified into two classes: medium-scale (MS) and large-scale (LS) waves, the features of which are indicated in Table 4 (Hocke and Schlegel, 1996).

Table 3
Selected satellite missions with in-situ ionospheric instruments (Yeh et al., 1999; Reigber et al., 1999; Le et al., 2003; Gwal et al., 2005; Rodrigues et al., 2009; Lin et al., 2017).

| Spacecraft | FORMOSAT-1 | CHAMP | DMSP F-16 |
|---|---|---|---|
| Duration | 1999 ~ 2004 | 2000 ~ 2010 | 2003 ~ |
| Orbit Altitude | 588 × 601 km | 450 km | 833 km |
| Inclination | 35° | 87.18° | 98.8° |
| SSO | X | X | O |
| Local Time | – | – | 20:03 |
| Payload | IPEI | DIDM | SSIES-3 |
| Science Data Sampling Rate | 2/16 Hz (IT: 32/1024 Hz) | 16 Hz (IT: 1/15 Hz) | 6 Hz (IT: 24 Hz) |
| Payload Mass | 9.26 kg | 2.2 kg | 96 kg |
| Spacecraft | DEMETER | C/NOFS | FORMOSAT-5 |
| Duration | 2004 ~ 2010 | 2008 ~ 2015 | 2017 ~ |
| Orbit Altitude | 710 km | 400 × 850 km | 720 km |
| Inclination | 98.23° | 13° | 98.28° |
| SSO | O | X | O |
| Local Time | 22:15 | – | 10:30/22:30 |
| Payload | IAP | IVM | AIP |
| Science Data Sampling Rate | 2.7 Hz (IT: 160 Hz) | 2 Hz (IT: 512 Hz) | 0.3/2.7/21.3 Hz (IT: 128/1024/8192 Hz) |
| Payload Mass | 50 kg | 70 kg | 4.5 kg |

The LSTIDs are observed as usually travelling from the poles to the equator after auroral disturbances during magnetic storms, but not always (Francis, 2003). On the other hand, MSTIDs can move parallel to the earth surface in guided wave-mode (Gossard and Hooke, 1975) as well as in free wave-mode (Francis, 1974). The theory of how AGWs interact with TIDs is far from being completed, the assumptions have not been confirmed experimentally and understood completely yet. The phase speed of LSTIDs is approximately 700 m/s (Pradipta et al., 2016), while the phase speed of MSTID is around 100–300 m/s (Hunsucker, 1982). The horizontal velocity of the MSTIDs is less than 0.25 km/s and that of the LSTID is 0.4–1000 km/s. The spacecraft is required to be able to measure the ion velocities cross track and in the ram direction within a range of ±2.5 km/s (cross track) and −7.5 ± 1 km/s (ram) at a sensitivity of ±10 m/s (cross track) and ±100 m/s (ram), with an accuracy of ±50 m/s (cross track) and ±200 m/s (ram). Since the CIP is oriented in the ram direction, relative to the CIP, the ion velocity is detected when the ions are moving into the ion trap. Therefore, the baseline velocity is negative. Owing to the high value of the spacecraft velocity relative to the phase velocities of MSTIDs and LSTIDs, the IDEASSat CIP will be able to provide a snapshot of the spatial structure of these irregularities.

The close relationship between Equatorial Plasma Bubbles (EPBs) and MSTIDs over South American Equatorial regions in July 2014 were observed by Takahashi et al. (2018). MSTIDs have been discussed as a possible source to generate plasma bubbles. There are two groups of MSTIDs classified by the different causes: (1) The MSTIDs generated via electrodynamical forces under the condition of the Perkins instability (Perkins, 1973). (2) The MSTIDs generated via atmospheric gravity waves propagating in the *F*-layer bottom side (Otsuka et al., 2013). However, the conditions and types of MSTIDs that are effective in generating EPBs are still unknown. To have a deeper understanding of the relationship between plasma bubbles and MSTIDs, it is useful to have stable long-term satellite-based observation during night-time to improve the current models.

Despite some speculation about the initiation of various plasma instabilities by AGWs, the relation between AGW and MSTID, day-to-day variability, zonal separation of plasma bubbles, and the relation between the electric fields driving vertical plasma drifts and the ionospheric *F* region wind dynamo are not understood. The multiple small satellites of the INSPIRE consortium carrying CIP will contribute to collecting additional data that will aid in the study of these phenomena.

### 2.3. Ionospheric planetary scale structure

Planetary-scale structures are defined as having wavelengths that are harmonics of the Earth's circumference. In the ionosphere, such planetary-scale structures can be the result of in-situ ionospheric processes such as photoionization, as well as vertical coupling from atmospheric tides and planetary waves (PWs) that propagate into the ionosphere from below (Chang et al., 2013a; Chang et al., 2013b; Chang et al., 2014).

Planetary wave type oscillations (PWTO) which are observed in ionospheric *F2*-layer parameters have been linked to middle atmospheric PWs (Borries and Hoffmann, 2010). Numerous observations show that global planetary-scale wavy perturbations having scale length larger than 1000 km exist in the ionosphere regularly (Aburjania et al., 2004). Sharadze et al. (1989) and Cavalieri et al. (1974) verified that the slow, long-period and large-scale waves present in the ionosphere, with phase velocities equal to local wind velocity, can have wavelengths of 1000–10,000 km and can last for a few days and longer.

The most dominant planetary waves in the winter stratosphere and mesosphere are Quasi-stationary planetary waves (QSPWs) (Liu and Richmond, 2013), QSPWs are usually constrained below the winter mesospause by critical layers formed by wind reversal (Smith, 1997). QSPWs can modulate atmospheric tides propagating upward from the lower atmosphere, which are capable of reaching ionospheric altitudes. PWs with multi-day periodicities are referred to as propagating planetary waves, and have also been linked to similar periodicities in ionospheric measurements (Chang et al., 2011; Gan et al., 2015).

PWs and atmospheric tides capable of propagating into the ionospheric E region can modulate vertical plasma drifts of the equatorial fountain formed by the wind dynamo mechanism. This allows for the periodicities and zonal wavenumbers of these PWs and atmospheric tides to be reflected in the ionospheric *F* region above. The effects of the E-region dynamo combined with transport effects in the *F* region is related to the wave-4 structure observed at high altitudes in ionosphere (Onohara et al., 2018). The wave-4 is defined as the four-peaked longitudinal structure that is a persistent feature of the low-latitude ionosphere system and is believed to be related to vertical coupling from the nonmigrating diurnal tide with eastward zonal wavenumber 3 (DE3) produced by tropospheric latent heat release (Immel et al., 2006; Chang et al., 2010). Atmospheric PWs and tides with long vertical wavelengths such as DE3 and ultra fast Kelvin waves are also capable of direct propagation into the ionospheric *F* region, allowing for direct modulation of the *F* region wind dynamo (Chang et al., 2010; Gasperini et al., 2015).

The global scale observations of IDEASSat will allow for the identification of such planetary-scale structures in the low latitude ionosphere.

### 2.4. Multi-platform INSPIRESat observations

As described above, measuring ionospheric variability requires observations of multiple plasma parameters at high sampling rates, as well as different local times,

latitudes, longitudes, and altitudes. As such, the ionosphere is well suited for observations using multiple small satellites and is one of the major scientific targets for small satellites developed by the INSPIRE consortium. The first small satellite project initiated by the INSPIRE consortium is INSPIRESat-1, which is a ~9U micosatellite being developed by the collaboration of NCU, CU, and IIST (Evonosky et al., 2018a). Leveraging the experience from participation in the development of the INSPIRESat-1 mission, a follow-on 3U CubeSat mission named IDEASSat (Ionospheric Dynamics Explorer and Attitude Subsystem Satellite)/INSPIRESat-2 (hereafter referred to as IDEASSat) was proposed by NCU in 2017, and was funded by the Taiwan National Space Organization (NSPO) and Ministry of Science and Technology (MOST) in Taiwan. Both INSPIRESat-1 and IDEASSat are carrying the Compact Ionospheric Probe (CIP), an in-situ multimode plasma sensor developed by NCU from heritage of the Advanced Ionospheric Probe (AIP) aboard the 450 kg FORMOSAT-5 satellite launched in 2017 (Lin et al., 2017). AIP and CIP are able to measure ion concentration, ion velocity, ion and electron temperature. FORMOSAT-5 AIP has been operational and returning nightside observations since September 2017. The top panel of Fig. 2 shows the ion density global distribution measured by FORMOSAT-5 AIP in November 2017 at 22:30 local time. The well-known wave-4 structure of the equatorial ionization anomalies is visible along the magnetic equator, with peaks over South America, Africa, Southeast Asia, and the Central Pacific (Immel et al., 2006).

INSPIRESat-1 is scheduled to be launched in May 2020 into a 500 km orbit, with the lifetime expected to be more than 1 year. IDEASSat is scheduled to be delivered in May 2020 for launch in Q4 2020. We therefore expect an overlap of at least 2–4 months for both spacecraft. In conjunction with INSPIRESat-1 and FORMOSAT-5, IDEASSat allows for mutlipoint in-situ measurements of the ionosphere using AIP and CIP, forming what has been termed the Smallsat Ionosphere Exploration at Several Times and Altitudes (SIESTA) constellation (Evonosky et al., 2018b).

As a 3U CubeSat, significant challenges that must be overcome in the design and operation of IDEASSat, include limited space, mass, and power margins. In the following sections, we describe the mission concept and system design of the IDEASSat spacecraft, as well as lessons learned throughout the development process.

Table 4
The parameters of MSTID and LSTID.

| | MSTID | LSTID |
|---|---|---|
| Wavelength (km) | 100–600 | >1000 |
| Temporal Period (h) | 0.25–1 | 0.5–4 |
| Horizontal Velocity (km/s) | <0.25 | 0.4–1000 |
| Phase Speed (m/s) | 100–300 | ~700 |

## 3. Mission architecture

The ionospheric F-region is located between 200 and ~1000 km altitude, dictating the orbit altitude range for a spacecraft performing in-situ measurements. A horizontal resolution of 20 km is needed to resolve ionospheric irregularities, corresponding to roughly half of the horizontal scale of a typical plasma bubble (Kil, 2015). Combined with an orbital velocity in the range of 7–8 km/s at these altitudes, this necessitates a sampling rate of at least 0.5–1 Hz for an in-situ plasma sensor. The latitude range shall exceed ±30°, in order to fully resolve the low latitude region where plasma bubbles occur, thereby imposing a minimum requirement on the orbit inclination. Finally, the mission lifetime is required to be longer than 6 months in order to resolve the seasonal variation of the ionosphere, but with de-orbit within 25 years to satisfy space debris mitigation guidelines. This imposes a range of valid orbital altitudes higher than 400 km based on reentry simulations using the Systems Tool Kit (STK) software from Analytical Graphics Inc (Saunders et al., 2009).

We have therefore selected a nominal 500 km Sun-synchronous orbit (97.41° inclination) with a local time of descending node (LTDN) between 10:00 and 12:00. Besides being more readily available in terms of secondary launch opportunities, the LTDN of the nominal orbit for IDEASSat is close to that of FORMOSAT-5 at 10:30, though the latter is at 720 km altitude. Combining observations from IDEASSat and FORMOSAT-5 will allow for taking measurements at similar orbit planes, but different altitudes, which will provide a much more comprehensive coverage of the ionosphere.

### 3.1. Science payload: Compact Ionospheric Probe

As mentioned previously, the payload for IDEASSat is the NCU-developed Compact Ionospheric Probe (CIP) - an in-situ plasma sensor that meets the ionospheric Science objectives of IDEASSat (Table 1). To function within a Cubesat, CIP is itself a miniaturized version of the Advanced Ionospheric Probe (AIP) carried aboard the FORMOSAT-5 spacecraft, which was launched in August 2017 (Lin et al., 2017). Both instruments are all-in-one sensors with four different measurement modes yielding the following ionospheric parameters:

- Planar Langmuir Probe (PLP): electron temperature.
- Ion Trap (IT): Ion density.
- Retarding Potential Analyzer (RPA): Light/ heavy ion mass ratio, ion temperature, ion ram speed.
- Ion Drift Meter (IDM): Ion arrival angles.

The mechanical structures of IDEASSat and CIP are shown in Fig. 3. The gold assembly on top of CIP corresponds to the Aperture and Meshes Module (AMM), which contains the PLP electrodes, grids and collectors for the three other modes, and a floating potential device,

which are exposed to the plasma environment. There are three printed circuit boards behind the AMM. These are the Analog Preprocessing Unit (APU), Digital Control Unit (DCU), and Power Management Unit (PMU). In order to satisfy the constraints of a CubeSat, the mass of CIP is 0.4 kg, with a volume of about 0.8U.

When in operation, the aperture of CIP is required to face in the direction of the spacecraft velocity vector. The instrument requires a Field Of View (FOV) that is a 90° angle centered about the velocity vector and originating at the perimeter edge of the CIP aperture plane. The uncertainty in pointing accuracy is required to be less than 0.5°, and the pointing knowledge uncertainty is required to be less than 0.1°.

The CIP measurement modes operate in a time sharing fashion. The ion velocity magnitude from RPA mode and the ion arrival angle in IDM mode can be combined to yield the relative ion velocity vector. There are 3 instrument modes for CIP: Safe, Normal, and Fast modes. In Safe mode, CIP will send 24 bytes of data containing the state of health (SOH) to the spacecraft command and data handling (C&DH) subsystem. The I-V curve sampling rates of CIP are different under Normal mode and Fast mode. In each mode, the raw data collected is in the form of voltage - current (I-V) curves sampled at 128 Hz in the Normal mode or 1024 Hz in the Fast mode. For 100% duty cycle, this results in a science data rate of 24.1 MB per day for Normal mode and 193.5 MB per day in Fast mode.

In both Normal and Fast mode, CIP typically cycles through three measurement modes every 3 s (PLP-RPA-IDM), returning 3 data packets in Normal mode, or 24 packets in Fast mode, from which the ionospheric parameters can be derived. This science data sampling rate of up to 8 Hz easily allows for horizontal resolution of ionospheric features with scales on the order of 1 km, thereby satisfying the previously mentioned mission objective with respect to ionospheric irregularities. Ancillary data appended to the science data packets formed by C&DH includes the following parameters: universal time (UT), spacecraft position, spacecraft velocity, and spacecraft attitude knowledge such as roll angle, pitch angle, and yaw angle in LVLH (Local Vertical Local Horizon) coordinate. By imposing a requirement for one month of onboard data storage, the onboard storage size for the IDEASSat C&DH is required to be larger than 5 GB.

### 3.2. Spacecraft

At a system level, IDEASSat is a 3U CubeSat that meets mass and volume constraints for most though not all CubeSat deployment modules. This is due to lateral protrusions and mass of just under 0.7 mm and 4.26 kg, respectively. These meet the CalPoly CubeSat Design Specifications of 0.9 mm and 4.5 kg (Mehrparvar et al., 2014). The C&DH and Electric Power Subsystem (EPS) have been developed by the INSPIRE team at NCU and IIST, while the deployable UHF tape measure antenna is also made in-house based on the Miniature X-ray Solar Spectrometer (MinXSS) Cubesat heritage design (Woods et al., 2013). Power requirements are satisfied with 4 Lithium ion batteries and 20 AzurSpace TJ 3G30A solar cells, with the latter arranged on two deployable and one body mounted solar panels. COTS components with prior flight heritage are utilized for spacecraft ADCS and communications subsystems, in order to satisfy development time and personnel constraints, as well as for risk mitigation. The fine pointing requirements of CIP are satisfied with a Blue Canyon Technologies (BCT) XACT ADCS with Global Positioning System (GPS) receiver (Mason et al., 2018). Data downlink as well as tracking telemetry and command (TT&C) uplink requirements are satisfied with a Clyde Space STXC-01-00031 S-Band Transmitter and a SpaceQuest TRX-U UHF Transceiver (Louw et al., 2016), respectively. The configuration of all subsystems in the mechanical structure

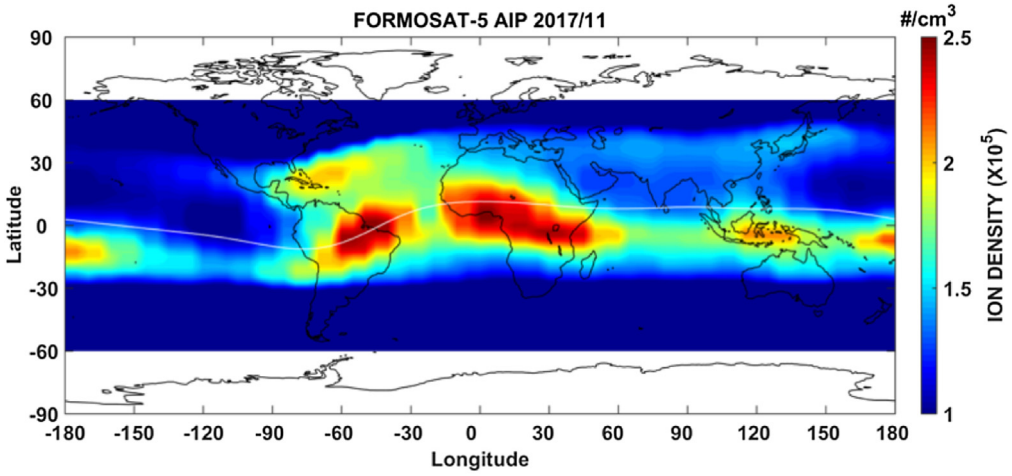


Fig. 2. The average ion density global distribution in 2017 November at 22:30 local time as observed by AIP.

is shown in the left panel of Fig. 3. The spacecraft coordinate system is defined with the CIP aperture pointing in the -Z direction, and the normal of the deployed and body mounted solar panels pointing in the -Y direction.

Internally, the EPS, C&DH and S-Band transmitter boards are arranged in a PC104 stack. The C&DH board includes connectors used for cable interfaces with other non-PC104 subsystems, including the UHF transceiver and ADCS. The batteries are attached to a separate module that includes a battery heater. The UHF tape measure antenna is deployed in the +Z direction. S-Band and GPS patch antennas are respectively attached to the −Y and +Y sides of IDEASSat. In a deployed state, the deployable and body mounted solar panels, as well as a coarse Sun sensor are located on the -Y side of the spacecraft.

### 3.3. Concept of operation

There are four modes of IDEASSat mission operation implemented in flight software (FSW): Phoenix mode, Safe mode, Charging mode and Science mode. Mode transitions are defined by the state of charge (SOC) of the spacecraft battery module, as well as ambient lighting conditions, as illustrated in Fig. 4. The transition SOCs in this figure are defined in a reconfigurable parameter table in FSW. All modes can only transition to adjacent modes according to the order denoted by the arrows in Fig. 4.

The states of the spacecraft subsystems in each mode are shown in Table 5. Emergency modes include Phoenix and Safe modes, and correspond to operation with minimal power draw to allow the batteries to recharge as quickly as possible. The Nominal modes are Charging and Science mode, which allow for a wider range of actions to be taken. Only C&DH, EPS and UHF Receiving will be as ON in every mode, and the UHF Transmitting function is always beaconing data packets containing state of health and tracking data for receipt by INSPIRE and amateur radio ground stations. The XACT ADCS is OFF in Phoenix mode, during which the spacecraft can be assumed to be tumbling. During Safe mode, the XACT ADCS is in Sun Point mode, which uses the coarse sensors as an absolute attitude reference to hold solar arrays pointing to the sun. During Nominal modes, the XACT ADCS is in Fine Reference Point mode, which is a high-performance mode for actual mission operations. CIP will only be ON during Science mode, and the S-band transmitter will be ON as required only in Nominal modes. The battery heater is always switched on as required.

Right after deployment and power on, the spacecraft will go into Phoenix mode. As the spacecraft tumbles with no ADCS, the deployable solar panels and UHF antenna are deployed using a thermal knife mechanism. Deployment attempts will continue periodically until the spacecraft is commanded to halt deployment by ground command.

After checking and configuring the EPS, the spacecraft will go to Safe mode if the state of charge (SOC) exceeds a threshold value currently set at 65%. If the SOC is lower than 55%, the spacecraft will go back to Phoenix mode. In Safe mode, the ADCS will be switched on and orient the coarse Sun sensor (CSS) and the solar cells on the -Y face towards the Sun in order to maximize the charging of the spacecraft batteries. In the event the UHF transceiver does not receive commands from a ground station for over a day, the FSW will assume that the TRX-U UHF transceiver is not working, and will perform a power cycle of the spacecraft. Although the spacecraft can transition between Safe to Phoenix mode autonomously, the spacecraft will go from Safe to Charging mode only with a command from a ground station when the SOC is higher than 75%, as denoted by the red arrow in Fig. 4. The spacecraft can go back to Safe mode without any command from the ground station when the SOC drops below 70%. This is intended to minimize risk in the event the spacecraft shifts unexpectedly from one of the Nominal modes to Safe mode.

During all modes except Phoenix mode, the XACT ADCS continuously provides FSW with spacecraft body rates, as well as the ambient lighting state. In Nominal operations, the spacecraft is in Charging mode on the Sunlit side, with the CSS and the solar cells oriented towards the Sun. The spacecraft transitions into Science mode during eclipse when SOC is higher than 85%, and orients the CIP aperture on the -Z face into the ram direction, allowing for plasma measurements to be made. As equatorial plasma bubbles are a nighttime phenomena, operating CIP during eclipse allows for measurements of these prominent scintillation causing irregularities. The spacecraft will go from Science mode to Charging mode when SOC is lower than 80% or when it is in sunlight. The standard of SOC values is updatable, depending on the healthy state of batteries as time goes by.

To execute this concept of operation, the IDEASSat team developed the spacecraft Flight Software (FSW) with the programming language C, and the hardware description language Verilog for the microprocessor on C&DH board.

The power consumption and generation per orbit in Table 6 is made under the assumption of operation under the Nominal modes. EPS, ADCS, GNSS, C&DH and UHF Receiving mode are operating at 100% duty cycle. UHF Transmitting mode is only 1.67%, while S-Band transmitting is 0.86%, and in standby mode for the other 99.14%. The CIP will be only operated at 40% duty cycle per orbit, while the solar panels are active for 60% corresponding respectively to the expected eclipse and sunlight ratios of the spacecraft orbit. The battery heater will be turned on for 10 s and rest for 60 s in eclipse in each mode as required to maintain the battery temperature in the operational region. The power consumption of battery heater is also included in the calculation.

### 3.4. Command and Data Handling Subsystem (C&DH) and Flight Software (FSW)

The C&DH of IDEASSat is comprised of a COTS Emcraft SmartFusion2 System-on-Module (M2S50-

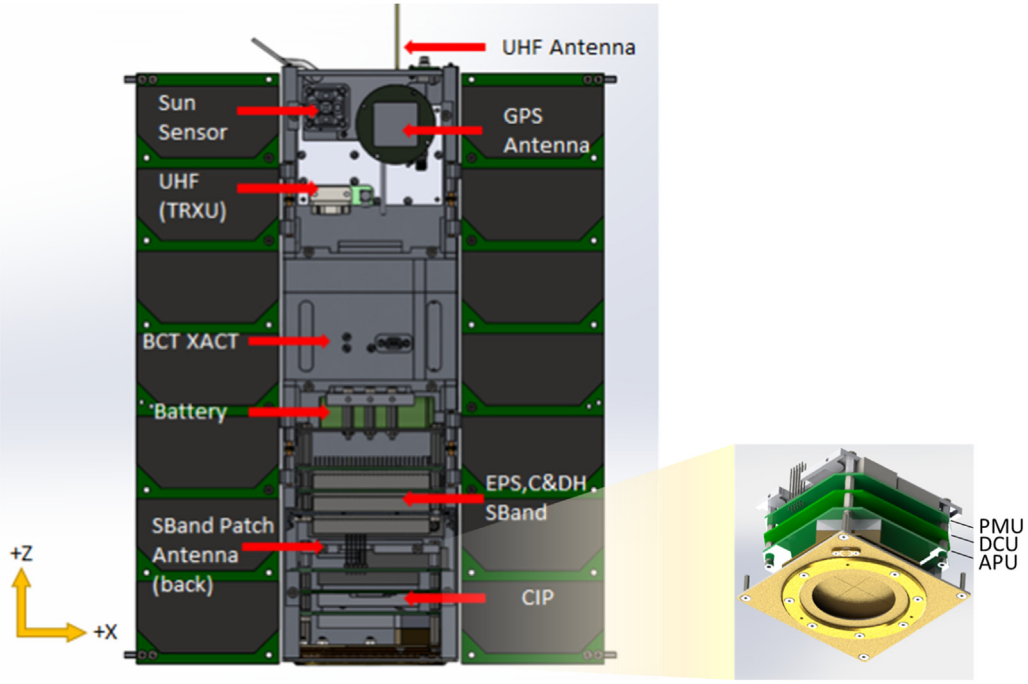


Fig. 3. The structures of IDEASSat (left) and CIP (right). The body mounted solar panel on the −y face is not shown, in order to elucidate the spacecraft interior. For CIP, APU is Analog Preprocessing Unit, DCU is Digital Control Unit, and PMU is Power Management Unit.

FG484 SOM), which includes a System-on-Chip (SoC) containing a microprocessor embedded in an FPGA. This is one of the lowest power consuming SOCs which contains a processor as well as an FPGA for flexibility of interfaces. The fully integrated Fight Software developed by IDEASSat team is written into the microprocessor and executed. To stack with EPS and S-band transmitter through a PC-104 interface, the SOC module is integrated to an interface card with a PC-104 connector sized according to that of the S-band transmitter. The C&DH interface card also includes pin socket connectors to the UHF, ADCS, GPS and GSE (Ground Support Equipment), which do not utilize the PC-104 interface. Data storage is on two redundant SD cards also located on the interface card.

To account for the possibility of variable data downlink access times for the spacecraft, the C&DH is required to store 3 months of data, necessitating an SD card larger than 18 GB. The SD-card sectors are allocated for each packet which is being sampled at the rates and sizes listed in Table 7. The Beacon packet contains the critical information about every subsystem which ground station can use to diagnose the spacecraft, and it will be downlinking through UHF band. The science packet contains the ionospheric data measured by CIP, and will be downlinked through S-band every time the spacecraft is in the access region above a ground station. The ADCS telemetry packet is provided by the BCT XACT. The information included in the ADCS telemetry packet are important for data retrieval according to the position and attitude condition when the science data were obtained. The ADCS image packet is provided by the star tracker, for attitude determination algorithm tests on the ground which meets the secondary mission objective described in Table 2. The Log packet is formed whenever some malfunction is detected by the flight software, it contains the message describing the malfunction.

The IDEASSat Flight Software (FSW) is FPGA-based software written in the programming language C and the hardware description language Verilog, installed on the On-Board Computer (OBC), which forms the spacecraft Command and Data Handling Subsystem (C&DH). The FSW is critical to mission success, both in development and execution. The main tasks to be performed by flight software are to check the state of each subsystem, recognize risks and handle emergencies autonomously when the spacecraft is out of contact with ground stations.

### *3.5. Attitude Determination and Control Subsystem (ADCS)*

For IDEASSat, attitude knowledge must be to within 0.1°, while attitude control must be to within 0.5° in order to satisfy the requirements of CIP. The ADCS subsystem controls the orientation of the spacecraft in space and tracks by updating the satellites orbital elements via the ADCS computer and GPS information. The ADCS subsystem for use in IDEASSat was procured from Blue Canyon Technologies (BCT). The BCT XACT is a self-contained ADCS with a suite of software controls and information available to the mission. It provides 3-axis stellar attitude determination in a 0.5U micro-package, as well as a CSS, magnetometers, and inertial measurement unit.

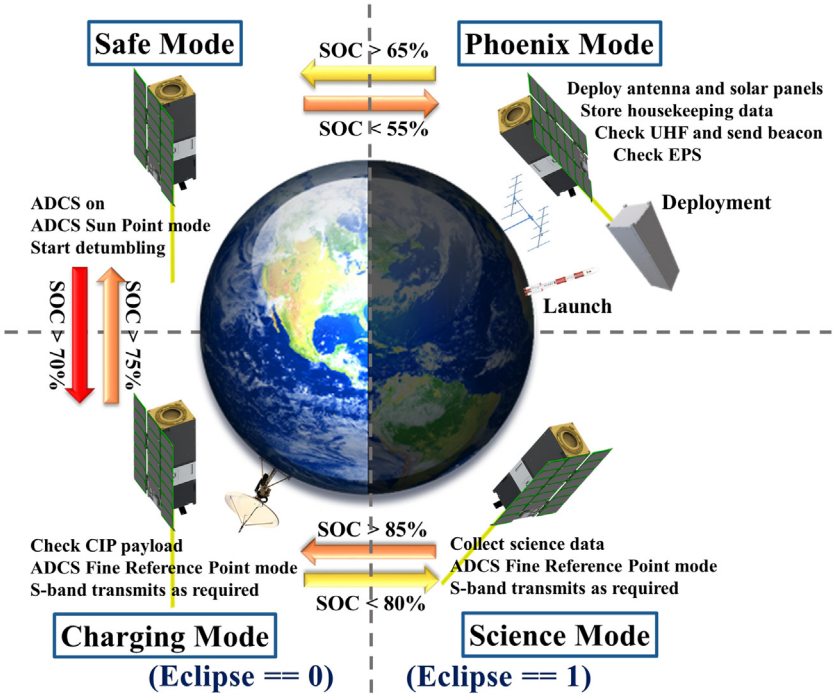


Fig. 4. The concept of operation of IDEASSat. Emergency mode includes Phoenix and Safe modes, and Nominal mode includes Charging and Science modes. Safe mode will only go to Charging mode with a command from ground stations, as denoted by the red arrow.

Table 5
IDEASSat Operational Modes.

| Subsystems | Emergency | | Nominal | |
|---|---|---|---|---|
| | Phoenix | Safe | Charging | Science |
| C&DH | ON | | | |
| EPS | ON | | | |
| ADCS | OFF | Coarse Sun | Fine Reference | |
| CIP | OFF | | | ON |
| UHF Rx | ON | | | |
| UHF Tx | Beacon | | | |
| S-Band Tx | OFF | | As Required | |
| Battery Heater | As Required | | | |

The star tracker points in the +X direction of the spacecraft frame. The XACT provides 3-axis attitude control with multiple pointing reference frames using three reaction wheels, as well as magnetorquers for detumble and momentum dumping. The XACT is TRL 9, having been flight qualified aboard the MinXSS spacecraft (Mason et al., 2017).

### 3.6. Electric Power Subsystem (EPS)

The IDEASSat EPS is comprised of two deployable solar panels, one body mounted solar panel, as well as a self-developed power control board, and a battery module.

#### 3.6.1. Solar cells and batteries

There are a total of 20 AzureSpace 3G30A solar cells (24.32 W) on the 3 panels, with a total cell area of 30.18 $cm^2$. In order to accommodate the CSS and ensure that the solar cells are exposed to maximum sunlight in ADCS coarse Sun pointing mode, the body mounted panel has 6 solar cells, as opposed to the 7 solar cells per panel on the deployable panels.

Sanyo NCR18650B-H00BA lithium ion batteries are selected for this mission, which are TRL 9. NCR18650B-H00BA cells have been used in multiple CubeSat missions, including NASA's GeneSat, SporeSat, O/OREOS and PharmaSat missions (Weston et al., 2018). 4 cells are used for the battery module, and are connected in two parallel

lines, each with two cells in series (2S2P) to supply the stable voltage as required. The battery module is sized to be same as the EPS power control board, and can handle cell balancing, as well as battery over charge protection.

### 3.6.2. Power generation

To design a suitable flight software sequence of operation, the battery SOC variation under each mode was simulated with charge/discharge calculations in MATLAB, with the objective of ensuring the spacecraft is power positive in all operational modes. The simulation setup for power consumption is indicated in Table 6. Considering the conversion efficiency of the solar panel regulator, the Nominal mode simulation was performed using a power draw of 3.5 W for CIP, 0.91 W for C&DH, 9 W for UHF Tx, 0.19 W for UHF Rx, 4.6 W for S-Band Tx and 6.1 W for the battery heater. In Safe mode, the EPS draws 3.08 W when charging and 0.22 W when it is not charging.

The SOC simulation for the spacecraft under Nominal operations after transitioning from Safe mode is shown in Fig. 5(a). The blue line corresponds to the variation of the battery SOC, while the orange line denotes the lighting state of the spacecraft, with sunlight indicated by high values and eclipse indicated by low values. The initial SOC at this transition point is 65%. The power requirements and duty cycles for this simulation are in accordance with the values shown previously in Table 6.

The simulation indicates that with the active attitude control for modes with battery SOC at Safe mode or above, the power balance is net positive and the spacecraft will not drop back to Phoenix after de-tumbling.

The SOC variation under the Emergency modes were also simulated to ensure that the spacecraft is capable of recovering from low charge conditions, and is shown in Figs. 5(b) and 5(c) for deployed and undeployed solar panels, respectively. The simulation of Phoenix mode is different from modes with higher SOC, because the spacecraft in Phoenix mode is still tumbling with ADCS powered down.

For de-tumbling analysis, a satellite attitude dynamics model was created. The model took into account the different disturbance torques arising from drag, solar radiation pressure, gravity gradient and magnetic dipole moment, and the initial spin rate was setup as 10 deg/s. The model utilizes Runge-Kutta 4th order integration scheme to propagate the attitude dynamics and kinematics equations (Schaub and Junkins, 2018). The initial SOC for these two simulations is assumed to be 60%. In Phoenix mode, the EPS draws 1.03 W when charging, and 0.1 W when it is not charging due to the efficiencies of buck converters utilized to regulate the solar panel voltage, as well as the DC-DC converters on the voltage outputs.

In Phoenix mode, the power draw for the battery heater is 6.1 W in Fig. 5 and 4.2 W in Fig. 5(c). Due to the power generation being most efficient when the solar panels are deployed and pointing directly to the Sun, the values are different for deployed and undeployed states. The simulation was set initially as 60% SOC, and can be seen from the Fig. 5, it does not drop lower than 50% in both of these situations. The SOC is slowly climbing after several orbits

Table 6
IDEASSat Nominal Power Consumption and Generation.

| Nominal Power Consumption (per orbit) | | |
|---|---|---|
| | Nominal (W) | Duty Cycle |
| Battery heater | 6.1 | Turn on 10(s) and rest 60(s) each time as required in eclipse. |
| EPS | Phx (Charging) 1.03<br>Phx (Uncharging) 0.1<br>Safe (Charging) 3.08<br>Safe (Uncharging) 0.22<br>Charging 3.08<br>Science 0.35 | 100.00% |
| ADCS | 2.82 | 100.00% except for Phx |
| GNSS | 0.90 | 100.00% except for Phx |
| C&DH | 0.91 | 100.00% |
| UHF Tx | 9.00 | Beacon<br>Phx & Safe: Rx 60 (s) & Tx 1(s)<br>Charging & Sci: Rx 30 (s) & Tx 1(s) |
| UHF Rx | 0.19 | Beacon<br>Phx & Safe: Rx 60 (s) & Tx 1(s)<br>Charging & Sci: Rx 30 (s) & Tx 1(s) |
| S-Band Tx | 4.60 | Access time over US&Taiwan&India |
| CIP | 3.5 | Eclipse |
| Nominal Power Generation (per orbit) | | |
| Solar Panels | 23.11 | 60.00% |

Table 7
SD card sizes and sectors per packet for different data packet types recorded by FSW.

| | Size (bytes) | NO. of sectors | Sampling Time (s) |
|---|---|---|---|
| Beacon | 223 | 1 | 1 |
| Science | 2291 | 5 | 1 |
| ADCS | 2061 | 5 | 30 |
| ADCS Image | 1749005 | 3417 | 20 |
| Log | 69 | 1 | Malfunction conditions |

which indicates that even under the Emergency modes, the SOC can still reach the 65% threshold to switch to Safe mode after a few orbits, and power up the ADCS to perform de-tumbling. Further simulations found that the lowest initial SOC value that will result in discharge to Phoenix mode levels is 60%.

### 3.7. Communications Subsystem (COMM)

The communications subsystem is required to receive uplinked commands from INSPIRE ground stations in Taiwan, Colorado, and India. COMM is further required to downlink science data from CIP and housekeeping data in the form of beacon packets. Beacon packets are intended for receipt both by INSPIRE ground stations, as well as the amateur radio community for tracking and SOH monitoring purposes. In the case of the latter, the telemetry definition of the beacon packets will be publicized. Following the operational concept of MinXSS, as well as other university small satellites operating on the amateur bands, reception reports from the amateur radio community will be encouraged through the distribution of QSL cards, as well as other memorabilia for frequently reporting stations (Mason et al., 2017).

Two bands will be used for telemetry purposes, the 70 cm UHF amateur band is for receiving commands from the INSPIRE ground stations and transmitting beacon packets, while the 13 cm amateur S-band will be used for downlinking the science data due to the higher bandwidth available. Commercial Off-the-Shelf (COTS) UHF transceivers and S-band transmitters are available that can satisfy our COMM requirements.

#### 3.7.1. UHF

The SpaceQuest (SQ) TRX-U transceiver is used for UHF communications on the spacecraft end, in conjunction with a monopole tape measure antenna. The monopole antenna is advantageous compared to a dipole antenna as the monopole only requires one deployable element, whereas the dipole requires two. This comes with the tradeoff of reduced antenna gain, due to the small area of the ground plane provided by small surface area of a 3U CubeSat.

Fig. 6 shows the Feldberechnung bei Korpern mit beliebiger Oberflache (FEKO) simulation of a quarter wave UHF tape antenna 3 dimensional radiation pattern assuming a ground plane corresponding to the IDEASSat structure. The peak gain is 6 dBi. The broad ominidirectional main lobe results in less stringent requirements of pointing direction to close the link budget, even in the event of a tumbling spacecraft.

The UHF telemetry of IDEASSat uses 9600 bits per second (bps) GMSK modulation with the AX.25 data link protocol. In ground tests, a National Instruments USRP-2900 software defined radio (SDR) was used to transmit a GMSK modulated signal at 9600 bps corresponding to the TRX-U sync word. If received successfully by the TRX-U, the sync word results in one of the pins of the TRX-U to be pulled high, and can be used in uplinked telemetry to distinguish real telemetry from spurious noise. During testing, the sync word was received and detected successfully by the TRX-U. During FlatSat tests and flight model functional tests, all commands and telemetry were transmitted to and from the spacecraft using the UHF radio link, in order to better represent actual operational conditions.

The use of the amateur bands by IDEASSat is subject to considerable uncertainty, both due to interference and frequency coordination reasons. In the case of the latter, spacecraft operating on the amateur bands are required by many regulatory agencies and launch providers to undergo frequency coordination by the International Amateur Radio Union (IARU). This process requires the submission of Advance Publication Information (API) to the International Telecommunications Union (ITU). This is not possible for IDEASSat as Taiwan is excluded from participation in the ITU due to political reasons (Lin, 2004). Due also to congestion on the UHF amateur bands, use of the 400.15–402 MHz band is being considered as a backup option. This band is allocated by both the Taiwan National Communications Commission (NCC) and the ITU Region 3 to meteorological and Earth exploration satellites, as well as space to Earth satellite communications and operations (Ministry of Transportation and Communications, 2017). Although this reduces the risk of interference and ensures voluntary compliance with IARU and ITU procedures, the tradeoff is a reduced number of ground stations available for beacon packet reception on non-amateur bands.

#### 3.7.2. S-band

For the S-band transmitter, the Clyde Space STXC transmitter developed by Cape Peninsula University of Technology (CPUT) is selected, which also satisfies related data downlink requirements. This PC/104 base module is TRL 9. The STXC is connected to the CPUT S-band antenna (SANT). SANT is a circularly polarized all metal patch antenna mounted on the +Y side of the spacecraft.

In the case of the S-band downlink, the downlink frequency was originally envisioned to be on the 13 cm amateur band, which is again subject to the difficulties of ITU and IARU registration for a Taiwanese satellite. Additionally, RF surveys near the NCU campus revealed significant

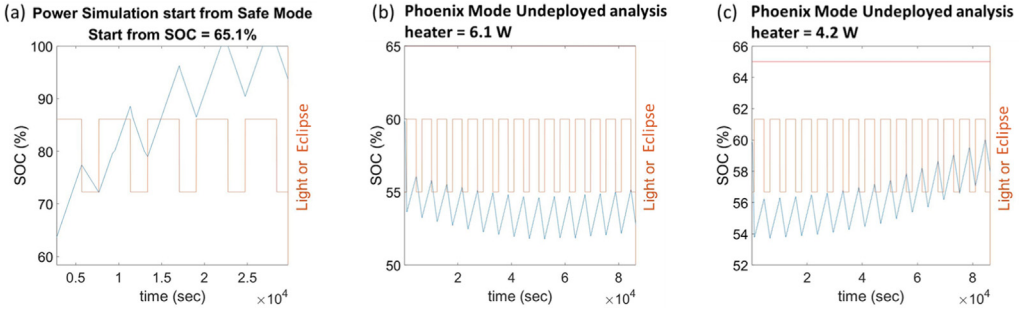


Fig. 5. Power simulation starts from (a) Safe mode with initial SOC = 65%, (b) initial SOC = 60% with battery heater drawing 6.1 W, then dropped below 55% and going into Phoenix mode directly before deploying solar panels, (c) initial SOC = 60% with battery heater drawing 4.2 W then below 55% and going into Phoenix mode directly before deploying solar panels. Blue line is battery SOC variation, and red line denotes lighting conditions, with low values corresponding to Eclipse and high values corresponding to sunlight.

interference in this band. As a result, downlink on the 2.2–2.290 GHz band was selected. This band is allocated by both the Taiwan NCC and ITU Region 3 to space research, space operation, and Earth exploration satellites (Ministry of Transportation and Communications, 2017). The housekeeping and science data transmitted via S-band will use The Consultative Committee for Space Data Systems (CCSDS) (CCSDS Secretariat, 2007) as an encoding standard and modulated by QPSK (quadrature phase shift keying).

Analyzing the access of IDEASSat to each ground station, the mission data downlinking capability is indicated in Table 8. The UHF Data rate is 9.6 kilobits per second (kbps), and the S-Band rate is 2 Megabits per second (Mbps), which is 0.25 Megabytes per second (MBps). However, for S-band, a 1 Mbps data rate is assumeed, as half-rate convolutional encoding is implemented. The access times to the ground stations are only considered for data downlink if they are longer than 5 min, due to the transceiving process requiring 1 min for connection establishment, 3 min for downlink data, and 1 min for command uplink. The average total daily access time is 83.40 min, the downlink data amount over both UHF and S-band is 308.69 Megabytes (MB), while during the Fast mode, with 40% CIP duty cycle, the data generation per day is 212.90 MB. Combining the Boulder, Taiwan, Singapore S-band ground stations, this is sufficient to downlink the expected CIP science data produced.

The ground side receiver system utilizes the USRP-2900 software defined radio (SDR) with signal processing and demodulation using GNU Radio, which is a free and open-source Python toolkit that provides signal processing blocks for SDR (Summers et al., 2018). A program in GNU Radio is shown as a flow graph constructed by blocks. Each block in GNU Radio corresponds to a different signal processing function, with the terminals at both ends of the flowchart indicating the input source and output sinks.

Fig. 7 is the flow graph of the Ground Station GNU Radio receiver system. The USRP source is connected with the ground station antenna via a low noise amplifier. The received signal is first low pass filtered to remove noise, with the cutoff frequency larger than half of the sampling rate. The clock recovery is applied for the purpose of ensuring that the receiver clock is properly aligned to the incoming data. The phase lock loop is applied to ensure that the input and output frequencies are the same, allowing for the phase of the signal to be effectively retrieved. To process the data received by the ground station, we perform QPSK demodulation with GNU radio and CCSDS decoding using spacecraft command software.

### 3.8. Structure

The structure of IDEASSat is mainly composed of aluminum (AL 6061-T6). The thickness of the walls is between 2 and 5 mm depending on location.

The Normal modes of the spacecraft are required to comply with requirements defined by the launch vehicle, in this case, the Indian Polar Satellite Launching Vehicle (PSLV). PSLV payload requirements dictate that the spacecraft fundamental frequency is required to be higher

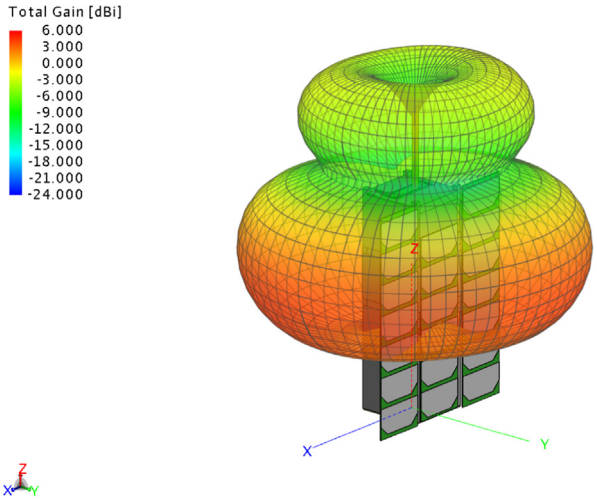


Fig. 6. Antenna pattern simulation of a quarter wave UHF antenna with ground plane using FEKO. The length of antenna is set as 17.14 cm in this simulation.

than 135 Hz. Frequency analysis for the spacecraft was performed using SolidWorks and the first 10 Normal mode frequencies computed, as shown in Fig. 8 The lowest Normal mode frequency was found to be 588.81 Hz, which complies with the PSLV requirements.

A static simulation of spacecraft structure was also performed, to determine the ability of the spacecraft structure to withstand launch loading. The maximum mass of a 3U CubeSat is required to be 4.00 kilograms according to the Cubesat Design Specification by Mehrparvar et al. (2014). The Factor of SAFEty (FOS) value indicates how much larger the maximum structural loading is relative to the expected load.

An FOS larger than 100 was defined as adequate margin. The results of the FOS simulation using SolidWorks is shown in Fig. 9. Dark blue colored regions indicate FOS values exceeding 100, accounting for nearly the entire spacecraft. The lowest FOS value found was 30, corresponding to a screw on the APU board in CIP.

### 3.9. Thermal Control Subsystem (TCS)

The main function of the thermal control subsystem is to ensure that all of the components on the satellite can be maintained within their operational temperature ranges in all modes and orbital attitudes.

Thermal analysis of the spacecraft on the component level was performed using Thermal Desktop to simulate the expected spacecraft temperatures under worst case cold (Phoenix mode eclipse), worst case hot (Charging mode sunlight) conditions, as well as Nominal operations. The results of the thermal simulations for these three conditions are shown in Table 4. It can be seen that the exposed solar panels experience the largest range of possible temperatures with a range of −51.86 °C to 65.73 °C. Subsystems contained entirely within the spacecraft chassis such as EPS and C&DH experience a much narrower range of temperatures, from 10.24 °C to 43.35 °C.

The temperature tolerances of the spacecraft subsystems are shown in Table 10. The solar panels temperature range is according to the experiments of relation between temperature of solar panels and power efficiency performed by Landis (1994) and Brandt et al. (2013). Comparing to the thermal simulation results in Table 9, it can be seen that all components are within an operational temperature range. Passive control mechanisms are preferred, owing to the limited power budget of the spacecraft. Components at risk of overheating were placed to maintain thermal contact with the spacecraft chassis in order to facilitate heat conduction.

## 4. Discussion

From the preceding analysis, it can be seen that the requirements of CIP can be satisfied using a 3U CubeSat. However, key challenges include the fine pointing knowledge and control requirements of CIP, the comparatively smaller area available for power generation on a 3U CubeSat, the buffer limitation of C&DH and FSW that causes the issue of data packets not being received by C&DH when the buffer is in the process of being cleared, as well as the large data volume and limited bandwidth of UHF communications.

In the case of the power constraint, this can be mitigated through the use of the Sun pointing mode of the XACT ADCS to maximize power generation capability. Conversely, power margins are extremely tight with the loss of ADCS capability in Phoenix mode and the resulting tumbling of the spacecraft. Although our simplified simulations show the spacecraft is still power positive in this state, this is dependent in large part on the nature of the tumbling motion, as well as changes to battery charging and power distribution efficiency at lower solar panel voltages and loads. In order to supply power in the most efficient way for a 3U CubeSat, Maximum power point tracking (MPPT) is applied to keep the charging state always efficient. The duty cycle of some components could be decreased in the worst case, and the electronic components on the EPS board with lower power consumption could be selected. For instance, the diode initially intended to prevent reverse charging of the solar cells by the battery during eclipse were replaced by Metal-Oxide-Semiconductor Field-Effect Transistors (MOSFETs).

Data from various subsystems transmitted to the C&DH are temporarily stored in a memory buffer. Initial Flat Sat tests showed that the C&DH was incapable of reading and clearing the memory buffer quickly enough when interfacing with high data rate subsystems such as CIP. To resolve this issue, the Ring buffer method was applied to the FSW to handle buffer read/ write functions. The ring buffer is a data structure that uses a single, fixed-size buffer as if it were connected end-to-end (Chandrasekaran, 2017). Using Ring buffer method, there is no need for buffer clearing, therefore the conflict is removed.

In the case of the data volume constraint, this is mitigated through the use of an S-band transmitter for science data downlink, at the cost of increased power draw, heating, and reduced space. Finally, the telecommunications licensing and frequency coordination process for IDEAS-Sat is complicated by Taiwan's exclusion from the ITU,

Table 8
Access and Data Downlink Details. 50% CIP duty cycle when it is in Fast mode.

| UHF Data rate | 9.6 kbps | S-Band rate | 0.125 MBps |
|---|---|---|---|
| Gnd St | Avg Access (>5 Min/Day) | UHF (MB/Day) | SBand (MB/Day) |
| Boulder, CO | 15.84 | – | 118.82 |
| IIST, India | 11.32 | 0.81 | – |
| NCU, Taiwan | 13.11 | – | 98.34 |
| NTU, Singapore | 11.80 | – | 88.47 |
| Muscat | 12.76 | 0.92 | – |
| Paris | 18.57 | 1.34 | – |
| Total | **83.40** | **3.07** | **305.62** |
| Data Gen/Day (MB, 40% CIP duty cycle) | | | **212.90** |

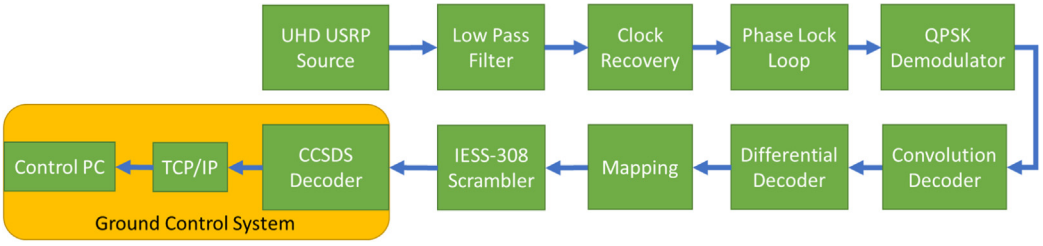


Fig. 7. The IDEASSat Ground Station S-band system diagram.

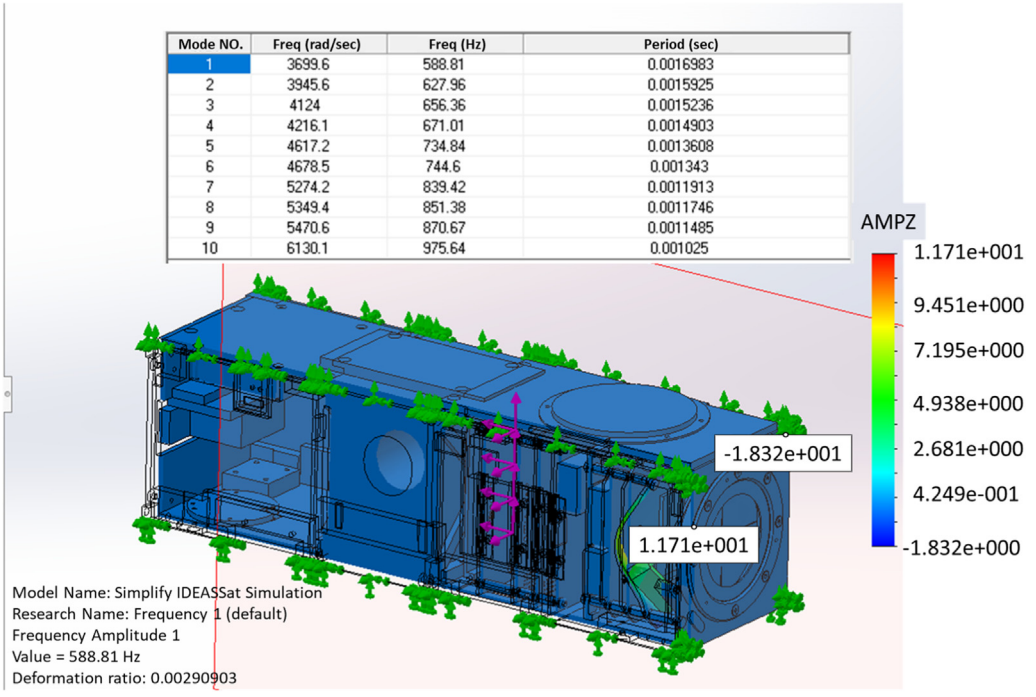


Fig. 8. Frequency analysis of IDEASSat spacecraft structure.

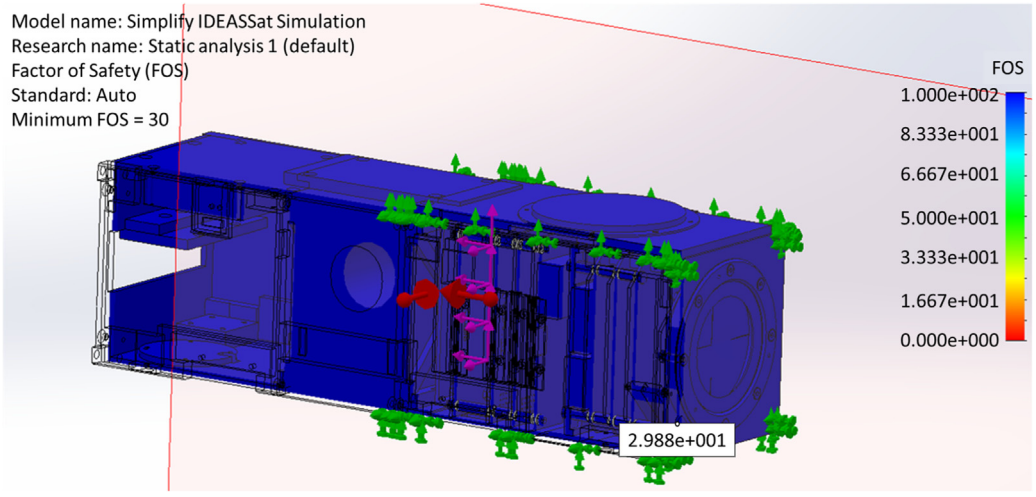


Fig. 9. The Factor of SAFEty (FOS) analysis in static simulation of IDEASSat spacecraft structure.

Table 9
Temperature ranges of each component with simulation of IDEASSat.

| Components | Worst Case Cold (°C) | Nominal(°C) | Worst Case Hot (°C) |
|---|---|---|---|
| Battery | 7.26–12.8 | 20.43–24.75 | 29.35–33.26 |
| EPS&C&DH | 10.24–27.79 | 24.25–34.93 | 39.61–43.35 |
| CIP | −2.23 to 19.25 | 17.53–26.46 | 31.78–38.83 |
| STXC | 4.17–20.64 | 18.65–27.29 | 30.14–37.28 |
| TRX-U | −3.82 to 14.12 | 10.41–22.73 | 30.46–34.22 |
| Solar Panels | −51.86 to 39.11 | −20.44 to 51.83 | 34.52–65.73 |

Table 10
Temperature tolerance range of each component.

| Subsystem | Component | Operating (°C) | Survival (°C) |
|---|---|---|---|
| CIP | CIP | −10 to 50 | −20 to 60 |
| ADCS | BCT XACT with GPS | −30 to 50 | −30 to 70 |
| COMM (UHF) | SQ TRX-U | −30 to 50 | −30 to 70 |
| COMM (S-Band) | CPUT STXC | −25 to 61 | −40 to 85 |
| EPS | Batteries | 5–35 | 0–40 |
| C&DH | C&DH PCB Board | −35 to 80 | −40 to 85 |
| Solar Panels | Solar Panels | −100 to 95 | −105 to 230 |

which limits access to launch providers, as well as the use of ground stations outside Taiwan.

The IDEASSat spacecraft integration commenced during May 2019, with testing during September 2019 through March 2020, and FM delivery in May 2020. Lessons learned during this phase have included the need for early prototyping, testing, and revision of self-developed hardware components. The amount of hardware debugging that can be accomplished without physical testing of a subsystem component was found to be extremely limited. Turnaround and delivery time for PCB fabrication and electrical components were also found to introduce considerable delays to the fabrication and testing process. Delivery times for several of the nano-D MILspec connectors required to interface with the COTS subsystems were found to be especially long, sometimes over two months. Combined with the high cost of such MILspec connectors, the EMs of several self-developed subsystems were designed to use more rapidly available micro-D connectors. While PCBs using the larger micro-D connectors were not compliant with the CubeSat volume constraints, the resulting EMs were still functional for functional testing and debugging, as well as FlatSat tests using single ended nano-D jumper cables.

## 5. Conclusions

The IDEASSat is a 3U CubeSat carrying the CIP payload with the mission objectives to study ionospheric variability, including structures on planetary scales and smaller scales on the order of 1 km. In this manuscript, we detail the feasibility study, concept of operations, and design of IDEASSat. This mission has benefited greatly through international collaboration via the INSPIRE consortium, and has served as a useful capacity building exercise for spacecraft engineering at NCU. The flight model of IDEASSat is scheduled to be delivered in May 2020, and launched in Q4 2020. Combined with AIP and CIP observations at different altitudes and local times from FORMOSAT-5 and INSPIRESat-1, IDEASSat will greatly expand observational capability for in-situ ionospheric measurements.

## Acknowledgement

This work is funded by Taiwan MOST grants 105-2111-M-008-001-MY3, 107-2111-M-008-002-MY3, 108-2636-M-008-002, and 109-2636-M-008-004, NSPO contract NSPO-S-106035, and Taiwan Ministry of Education Higher Education Deep Cultivation Project support for the NCU Center for Astronautical Physics and Engineering. The authors gratefully acknowledge the worldwide members of the INSPIRE consortium for their continued efforts and support, as well as Wengang Zheng, Rick Kohnert, Gail Tate, and Ed Wullschleger of the Laboratory for Atmospheric and Space Physics, University of Colorado at Boulder for their assistance and support.

NCU acknowledges software support and academic licensing from the Analytical Graphics, Incorporated (AGI) Educational Alliance Program, as well as C&R Technologies.

## References

Aburjania, G.D., Chargazia, K.Z., Jandieri, G.V., Khantadze, A.G., Kharshiladze, O.A., 2004. On the new modes of planetary-scale electromagnetic waves in the ionosphere. Ann. Geophys. 22, 1203–1211, doi: 1432-0576/ag/2004-22-1203.

Afraimovich, E.L., Astafieva, E.I., Voyeikov, S.V., 2004. Isolated ionospheric disturbances as deduced from global GPS network. Ann. Geophys. 22 (1), 47–62. https://doi.org/10.5194/angeo-22-47-2004.

Baker, D.N., Chandran, A., 2018. Space, still the final frontier. Science. 361(207), Iss. 6399, pp. 207, doi: 10.1126/science.aau7631.

Berthelier, J.J., Godefroy, M., Leblanc, F., Seran, E., Peschard, D., Gilbert, P., Artru, J., 2006. IAP, the thermal plasma analyzer on DEMETER. Planet. Space Sci. 54 (5), 487–501.

Borries, C., Hoffmann, P., 2010. Characteristics of F2-layer planetary wave–type oscillations in northern middle and high latitudes during 2002 to 2008. J. Geophys. Res. 115, A00G10. https://doi.org/10.1029/2010JA015456.

Brandt, C., Baur, C., Caon, A., Müller-Buschbaum, P., Zimmermann, C., Andreev, T., 2013. The influence of high temperatures on radiation damage of GaInP2/GaAs/Ge triple junction cells. IEEE J. Photovoltaics 3 (2), 904–908. https://doi.org/10.1109/JPHOTOV.2013.2242958.

Cavalieri, D.J., Deland, R.J., Potemra, T.A., Gavin, R.F., 1974. The correlation of VLF propagation variations with atmospheric planetary-scale waves. J. Atmos. Terr. Phys. 36, 561–574.

CCSDS Secretariat, Office of Space Communication (Code M-3), National Aeronautics and Space Administration (2007), Recommendation for Space Data System Standards: CCSDS FILE DELIVERY PROTOCOL (CFDP), Recommended Standard CCSDS 727.0-B-4, Blue Book, Issue 4.

Chandrasekaran, S., 2017. Implementing Circular/Ring Buffer in Embedded C, Embed Journal, EmbedJournal Team, Retrieved 14 August 2017.

Chang, L.C., Palo, S.E., Liu, H.-L., Fang, T.-W., Lin, C.S., 2010. Response of the thermosphere and ionosphere to an ultra fast Kelvin wave. J. Geophys. Res. 115, A00G04. https://doi.org/10.1029/2010JA015453.

Chang, L.C., Liu, J.-Y., Palo, S.E., 2011. Propagating planetary wave coupling in SABER MLT temperatures and GPS TEC during the 2005/2006 austral summer. J. Geophys. Res. 116, A10324. https://doi.org/10.1029/2011JA016687.

Chang, L.C., Lin, C.-H., Liu, J.-Y., Balan, N., Yue, J., Lin, J.-T., 2013a. Seasonal and local time variation of ionospheric migrating tides in 2007–2011 FORMOSAT-3/COSMIC and TIE-GCM total electron content. J. Geophys. Res. Space Phys. 118, 254–2564. https://doi.org/10.1002/jgra.50268.

Chang, L.C., Lin, C.-H., Yue, J., Liu, J.-Y., Lin, J.-T., 2013b. Stationary planetary wave and nonmigrating tidal signatures in ionospheric wave 3 and wave 4 variations in 2007–2011 FORMOSAT-3/COSMIC observations. J. Geophys. Res. Space Phys. 118, 6651–6665. https://doi.org/10.1002/jgra.50583.

Chang, L.C., Yue, J., Wang, W., Wu, Q., Meier, R.R., 2014. Quasi-two day wave related variability in the background dynamics and composition of the mesosphere/thermosphere, and the ionosphere. J. Geophys. Res. Space Phys. 119, 4786–4804. https://doi.org/10.1002/2014JA019936.

Chang, L.C., Chao, C.-K., Kuo, C.-L., Liu, J.-Y., Duann, Y., Chandran, A., Fang, T.-W., Priyadarshan, H., Kaustubh, A.K., Evonosky, W., 2018a. IDEASSat: the ionosphere dynamics explorer and attitude subsystem satellite. In: SSC18-WKIV-06, Proceedings of the 32nd Annual AIAA/USU Conference on Small Satellites, Logan, UT, USA.

Chang, L.C., Chao, C.K., Chandran, A., Kuo, C.-L., Liu, J.-Y., Duann, Y., Chiu, Y.-C., Tsai-Lin, R., Luo, W.-H., Tai, T.-Y., Liao, C.-T., Liu, H.-T., Chung, C.-J., Duann, R., Yang, Z.-M., 2018b. IDEASSat – A 3U CubeSat for ionospheric science and capacity building. In: IAC-18-B4.2.6, 69th International Astronautical Congress (IAC), Bremen, Germany, 1–5 October 2018.

Daniel, A., Tilahun, G., Teshager, A., 2016. Effect of ionosphere on radio wave propagation. Int. J. Res. 3(9), e-ISSN: 2348-795X.

Evonosky, W., Chandran, A., Boyajian, S., Priyadarshan, H., Verma, A., Niwhashini, N., Kaustubh, K., Chang, L., Duann, Y., Mao, Y.-C., Tsai-Lin, R., Chiu, S.-C., 2018a. INSPIRESat-1: an ionosphere exploring Microsat, SSC18-WKIV-04. In: Proceedings of the 32nd Annual AIAA/USU Conference on Small Satellites, Logan, UT, USA, 2018, 4–9 August.

Evonosky, W., Boyajian, S., Duann, Y., Tsai-Lin, R., Chen, Y.C., Chung, C.J., Mao, Y.C., Kandi, K., Verma, A., Nandagopan, N., Viyayawat, S., Palo, A., 2018b. Smallsat ionosphere exploration at several times and altitudes (SIESTA). In: The Sixth UNISEC-Global Meeting, November 19-21, 2018, Strasbourg, France.

Francis, S.H., 1974. A theory of medium-scale traveling ionospheric disturbances. J. Geophys. Res. 79 (34), 5245–5260.

Francis, S.H., 2003. Global propagation of atmospheric gravity waves: a review. J. Atmos. Terr. Phys. 37 (6–7), 1011–1030. https://doi.org/10.1016/0021-9169(75)90012-4.

Fedorenko, Y.P., Tyrnov, O.F., Fedorenko, V.N., Dorohov, Vasiliy L., 2013. Model of traveling ionospheric disturbances. J. Space Weather Space Clim. 3 (A30). https://doi.org/10.1051/swsc/2013052.

Frissell, N.A., Miller, E.S., Kaeppler, S.R., Ceglia, F., Pascoe, D., Sinanis, N., Smith, P., Williams, R., Shovkoplyas, A., 2014. Ionospheric sounding using real-time amateur radio reporting networks. Space Weather 12, 651–656. https://doi.org/10.1002/2014SW001132.

Gossard, E.E., Hooke, W.H., 1975. Waves in the Atmosphere. Elsevier, Amsterdam, Netherlands, p. 456.

Gan, Q., Yue, J., Chang, L.C., Wang, W.B., Zhang, S.D., Du, J., 2015. Observations of thermosphere and ionosphere changes due to the dissipative 6.5-day wave in the lower thermosphere. Ann. Geophys. 33 (7), 913–922. https://doi.org/10.5194/angeo-33-913-2015.

Gasperini, F., Forbes, J.M., Doornbos, E.N., Bruinsma, S.L., 2015. Wave coupling between the lower and middle thermosphere as viewed from TIMED and GOCE. J. Geophys. Res. Space Phys. 120, 5788–5804. https://doi.org/10.1002/2015JA021300.

Gwal, A.K., Parrot, M., Pincon, J.L., Lebreton, J.P., Trigunait, A., Sarkar, S., Malhotra, K., Sharma, N., 2005. Variation of electron density above india observed by DEMETER microsatellite and the CRABEX project. In: Proceedings of the XXVIIIth URSI General Assembly, October 2005, New Delhi, India.

Hocke, K., Schlegel, K., 1996. A review of atmospheric gravity waves and traveling ionospheric disturbances: 1982–1995. Ann. Geophys. 14, 917–940.

Hunsucker, R.D., 1982. Atmospheric gravity waves generated in the high-latitude ionosphere: a review. Rev. Geophys. 20(2), 293-315. ISSN 1944-9208. 1, 5, 127, 129.

Immel, T.J., Sagawa, E., England, S.L., Henderson, S.B., Hagan, M.E., Mende, S.B., Frey, H.U., Swenson, C.M., Paxton, L.J., 2006. Control of equatorial ionospheric morphology by atmospheric tides. Geophys. Res. Lett. 33 (15). https://doi.org/10.1029/2006GL026161.

International Amatuer Radio Union, Amateur Radio Satellite Frequency Coordination, retrieved from: http://www.iaru.org/amateur-radio-satellite-frequency-coordination.html.

International Telecommunications Union, ITU filing procedures for small satellites, retrieved from: https://www.itu.int/en/ITU-R/space/Pages/supportSmallSat.aspx.

Kihn, E.A., Redmon, R., Ridley, A.J., Hairston, M.R., 2006. A statistical comparison of the AMIE derived and DMSP-SSIES observed high-latitude ionospheric electric field. J. Geophys. Res. 111, A08303. https://doi.org/10.1029/2005JA011310.

Kelly, M.A., Comberiate, J.M., Miller, E.S., Paxton, L.J., 2014. Progress toward forecasting of space weather effects on UHF SATCOM after Operation Anaconda. Space Weather 12, 601–611. https://doi.org/10.1002/2014SW001081.

Kil, H., 2015. The morphology of equatorial plasma bubbles - a review. J. Astron. Space Sci. 32, 13–19. https://doi.org/10.5140/JASS.2015.32.1.13.

Kil, H., Kwak, Y.-S., Lee, W.K., Miller, E.S., Oh, S.-J., Choi, H.-S., 2015. The causal relationship between plasma bubbles and blobs in the low-latitude F region during a solar minimum. J. Geophys. Res. Space Phys. 120, 3961–3969. https://doi.org/10.1002/2014JA020847.

Landis, A.G., 1994. Review of solar cell temperature coefficients for space. In: Proceedings of the XIII Space Photovoltaic Research and Technology Conference (SPRAT XIII). NASA CP-3278, published by NASA, Washington, D.C., 1994, pp. 385.

Le, G., Huang, C.-S., Pfaff, R.F., Su, S.-Y., Yeh, H.-C., Heelis, R.A., Rich, F.J., Hairston, M., 2003. Plasma density enhancements associated with equatorial spread F: ROCSAT-1 and DMSP observations. J. Geophys. Res. 108 (A8), 1318. https://doi.org/10.1029/2002JA009592.

Lin, C.-H., 2004. International telecommunications union and the Republic of China (Taiwan): prospects of Taiwan's participation,

Ann. Surv. Int. Comparat. Law, 10-1, 133–164. Available at: https://digitalcommons.law.ggu.edu/annlsurvey/vol10/iss1/6.

Louw, E., Jooste, C., Steenkamp, L., 2016. User manual STXC-01-00031. No. USM-01-00031. Rev B. Cape Peninsula University of Technology, French South African Institute of Technology.

Lin, Z.W., Chao, C.K., Liu, J.Y., Huang, C.M., Chu, Y.H., Su, C.L., Mao, Y.C., Chang, Y.S., 2017. Advanced Ionospheric Probe scientific mission onboard FORMOSAT-5 satellite. Terr. Atmos. Ocean. Sci. 28, 99–110. https://doi.org/10.3319/TAO.2016.09.14.01(EOF5).

Liu, H.-L., Richmond, A.D., 2013. Attribution of ionospheric vertical plasma drift perturbations to large-scale waves and the dependence on solar activity. J. Geophys. Res. Space Phys. 118, 2452–2465. https://doi.org/10.1002/jgra.50265.

Mehrparvar, A., Pignatelli, D., Carnahan, J., Munakata, R., Lan, W., Toorian, A., Hutputanasin, A., Lee, S., 2014. CubeSat Design Specification Rev. 13, The CubeSat Program. Cal Poly SLO.

Merlino, R.L., 2007. Understanding Langmuir probe current-voltage characteristics. Am. J. Phys. 75 (12), 1078–1085. https://doi.org/10.1119/1.2772282.

Mason, J.P., Lamprecht, B., Downs, C., Woods, T.N., 2018. CubeSat on-orbit temperature comparison to thermal-balance-tuned model predictions. J. Thermophys. Heat Transf. 32 (1), 237–255. https://doi.org/10.2514/1.T5169.

Mason, J.P., Baumgart, M., Rogler, B., Downs, C., Williams, M., Woods, T.N., Palo, S., Chamberlin, P.C., Solomon, S., Jones, A., Li, X., Kohnert, R., Caspi, A., 2017. MinXSS-1 CubeSat on-orbit pointing and power performance: the first flight of the blue canyon technologies XACT 3-axis attitude determination and control system. J. Small Satellites 6 (3), 651–662.

Ministry of Transportation and Communications, 2017, Table of Radio Frequency Allocations of the Republic of China, 2017.2 Revised, retrieved from: https://freqdbo.ncc.gov.tw/Portal/NCCB03F_.aspx.

Ogawa, T., Balan, N., Otsuka, Y., Shiokawa, K., Ihara, C., Shimomai, T., Saito, A., 2001. Observations and modeling of 630 nm airglow and total electron content associated with traveling ionospheric disturbances over Shigaraki, Japan. Earth, Planets Space 54 (1), 45–56. https://doi.org/10.1186/BF03352420.

Onohara, A.N., Batista, I.S., Batista, P.P., 2018. Wavenumber-4 structures observed in the low-latitude ionosphere during low and high solar activity periods using FORMOSAT/COSMIC observations. Ann. Geophys. 36, 459–471. https://doi.org/10.5194/angeo-36-459-2018.

Otsuka, Y., Suzuki, K., Nakagawa, S., Nishioka, M., Shiokawa, K., Tsugawa, T., 2013. GPS observations of medium-scale traveling ionospheric disturbances over Europe. Ann. Geophys. 31, 163–172. https://doi.org/10.5194/angeo-31-163-2013.

Perkins, F., 1973. Spread F and ionospheric currents. J. Geophys. Res. 78 (1), 218–226. https://doi.org/10.1029/JA078i001p00218.

Pradipta, R., Valladares, C.E., Carter, B.A., Doherty, P.H., 2016. Interhemispheric propagation and interactions of auroral traveling ionospheric disturbances near the equator. J. Geophys. Res. Space Phys. 121, 2462–2474. https://doi.org/10.1002/2015JA022043.

Reifman, A., Dow, W.G., 1949. Dynamic probe measurements in the ionosphere. Phys. Rev. 76, 987–988. https://doi.org/10.1103/PhysRev.76.987.

Reigber, Ch., Schwintzer, P., Lühr, H., 1999. The CHAMP geopotential mission. Bollettino di Geofisica Teorica ed Applicata 40 (3–4), 285–289.

Reigber, Ch., Lühr, H., Schwintzer, P., Potsdam, G., 2001. Announcement of Opportunity for CHAMP, GFZ Helmholtz Centre Potsdam, CH-GFZ-AO-001.

Retterer, J.M., 2010. Forecasting low-latitude radio scintillation with 3-D ionospheric plume models: 1. Plume model. J. Geophys. Res. 115, A03306. https://doi.org/10.1029/2008JA013839.

Rodrigues, F.S., Kelley, M.C., Roddy, P.A., Hunton, D.E., Pfaff, R.F., de La Beaujardiere, O., Bust, G.S., 2009. C/NOFS observations of intermediate and transitional scale-size equatorial spread F irregularities. Geophys. Res. Lett. 36 (18), L00C05. https://doi.org/10.1029/2009GL038905.

Saunders, A., Lewis, H., Swinerd, G.G., 2009. A new tool for satellite re-entry predictions, European Space Agency, (Special Publication) ESA SP. 672, retrieved from: https://conference.sdo.esoc.esa.int/proceedings/sdc5/paper/20.

Sharadze, Z.S., Mosashvili, N.B., Pushkova, G.N., Judovich, L.A., 1989. Long-period wave disturbances in E-region of the ionosphere. Geomag. Aeron. 29, 1032–1035.

Schaub, H., Junkins, J.L., 2018. Analytical Mechanics of Space Systems, AIAA Education Series, fourth ed. American Institute of Aeronautics and Astronautics, Reston, VA, USA. ISBN-10: 1624105211.

Smith, A.K., 1997. Stationary planetary waves in upper mesospheric winds. J. Atmos. Sci. 54 (16), 2129–2145. https://doi.org/10.1175/1520-0469(1997) 054<2129:SPWIUM>2.0.CO;2.

Stoneback, R.A., Heelis, R.A., Burrell, A.G., Coley, W.R., Fejer, B.G., Pacheco, E., 2011. Observations of quiet time vertical ion drift in the equatorial ionosphere during the solar minimum period of 2009. J. Geophys. Res. 116, A12327. https://doi.org/10.1029/2011JA016712.

Su, S.-Y., Yeh, H.C., Heelis, R.A., 2001. ROCSAT 1 ionospheric plasma and electrodynamics instrument observations of equatorial spread F: an early transitional scale result. J. Geophys. Res. 106 (A12), 29153–29159. https://doi.org/10.1029/2001JA900109.

Sultan, P.J., 1996. Linear theory and modeling of the Rayleigh-Taylor instability leading to the occurrence of equatorial spread F. J. Geophys. Res. 101 (A12), 26875–26891. https://doi.org/10.1029/96JA00682.

Summers, T., Schmandt, J., Cheung, E., Gentry, C., Chen, Y., 2018. Cost effective, flexible ground architecture using software defined radio and GNU Radio. In: SSC18-X-03, Proceedings of the 32nd Annual AIAA/USU Conference on Small Satellites, Logan, UT, USA, 2018, 4–9 August.

Takahashi, H., Wrasse, C.M., Figueiredo, C.A.O.B., Barros, D., Abdu, M.A., Otsuka, Y., Shiokawa, K., 2018. Equatorial plasma bubble seeding by MSTIDs in the ionosphere. Prog. Earth Planet. Sci. 5 (32). https://doi.org/10.1186/s40645-018-0189-2.

Teillet, P.M., Gauthier, R.P., Chichagov, A., 2003. Towards Integrated Earth Sensing: The Role of In Situ Sensing in Real-time, Information Technology for Future Intelligent Earth Observing Satellites. Hierophantes Publishing Services, Pottstown, PA, USA, ISBN: 0-9727940-0-X.

Weston, S., Agasid, E., Burton, R., Carlino, R., Defouw, G., Perez, A.D., Karacalıoglu, A.G., Klamm, B., Rademacher, A., Schalkwyck, J., Shimmin, R., Tilles, J., 2018. State of the Art: Small Spacecraft Technology, NASA/TP–2018–220027. Retrieved from: https://www.nasa.gov/sites/default/files/atoms/files/soa2018_final_doc.pdf.

Woods, T.N., Caspi, A., Chamberlin, P., Jones, A., Konert, R., Li, X., Palo, S., Solomon, S., 2013. MinXSS - Miniature X-ray Solar Spectrometer (MinXSS) CubeSat Mission, Submitted to NASA. Retrieved from: https://www.pinheadinstitute.org/wp-content/uploads/2014/07/MinXSS_Proposal2013_NASA.pdf.

Yeh, H.C., Su, S.Y., Yeh, Y.C., Wu, J.M., Heelis, R.A., Holt, B.J., 1999. Scientific mission of the IPEI payload onboard ROCSAT-1. Terr. Atmos. Ocean. Sci. 10 (1), 19–42. https://doi.org/10.3319/TAO.1999.10.S.19(ROCSAT).

Zhong, P., Ding, X.L., Zheng, D.W., Chen, W., Huang, D.F., 2008. Adaptive wavelet transform based on cross-validation method and its application to GPS multipath mitigation. GPS Solut. 12, 109–117. https://doi.org/10.1007/s10291-007-0071-y.